Research Square

Preprints are preliminary reports that have not undergone peer review.
They should not be considered conclusive, used to inform clinical practice,
or referenced by the media as validated information.

OTUD3 Deubiquitinates PLD1 to Modulate Neurodevelopment and Cognitive Function

Qian Jiao

jiaoqian@qdu.edu.cn

Qingdao University

Tongying Xu

Qingdao University

Yao Chen

Qingdao University

Qiqi Zhao

Qingdao University

Kaiyue Ren

Qingdao University

Liu Yuhan

Qingdao University

shuo Liu

https://orcid.org/0000-0003-1446-6955

Yu Zhong

Qingdao University

Dang Xiaoting

University of Health and Rehabilitation Sciences

Xuejie Huan

Qingdao University

Zhengyang Yao

Qingdao University

Fengju Jia

Qingdao University

Hong Jiang

University of Health and Rehabilitation Sciences

Article

Keywords: OTUD3, brain development, neural stem/progenitor cells, deubiquitinase, PLD1, lipid metabolism, synaptic homeostasis

Posted Date: November 24th, 2026

DOI: https://doi.org/10.21203/rs.3.rs-11439023/v1

License: This work is licensed under a Creative Commons Attribution 4.0 International License.
Read Full License

Additional Declarations:
(Not answered)

Table 1 is available in the Supplementary Files section.

OTUD3 Deubiquitinates PLD1 to Modulate Neurodevelopment and Cognitive Function

Tongying Xu[1#], Yao Chen[1#], Qiqi Zhao[1#], Kaiyue Ren[1#], Yuhan Liu[1], Shuo Liu[1], Yu Zhong[1], Xiaoting Dang[2], Xuejie Huan[2], Zhengyang Yao[1], Fengju Jia[3], Qian Jiao[1*], Hong Jiang[2*]

1. Department of Physiology, Shandong Key Laboratory of Pathogenesis and Prevention of Brain Diseases and State Key Disciplines: Physiology, School of Basic Medicine, Qingdao Medical College, Qingdao University, Qingdao, 266071, China.
2. Shandong Key Laboratory of Neurorehabilitation, University of Health and Rehabilitation Sciences, Qingdao, 266113, China.
3. School of Nursing, Qingdao University, Qingdao, 266071, China

*Corresponding author: Hong Jiang: jianghong@uhrs.edu.cn; Qian Jiao: jiaoqian@qdu.edu.cn.
# These authors contributed equally to this work

Abstract

OTUD3 is a deubiquitinase with poorly characterized roles in mammalian neurodevelopment. Here, we show that OTUD3 is enriched in neurons in the developing brain and is aberrantly expressed in human neurodegenerative diseases. *Otud3* knockout mice exhibit severe cognitive deficits, reduced brain size, and thinner cerebral cortices. Intriguingly, *Otud3* transgenic overexpression similarly impairs cortical morphogenesis, underscoring that precise regulation of OTUD3 dosage is essential for normal brain development. Mechanistically, OTUD3 cell-autonomously inhibits neural stem/progenitor cells (NS/PCs) proliferation, promotes apoptosis and delays neuronal differentiation. Quantitative proteomics reveals stage-specific dysregulation in *Otud3* knockout brains: cell cycle and DNA replication pathways are disrupted at early embryonic stages, whereas lipid metabolism and synaptic signaling are suppressed at post-differentiation stages. We identify phospholipase D1 (PLD1) as a substrate of OTUD3 and demonstrate that OTUD3 stabilizes PLD1 through deubiquitination, preserving PLD1 enzymatic activity and synaptic protein homeostasis. PLD1 re-expression rescues lipid signaling deficits caused by OTUD3 depletion. Collectively, our findings establish OTUD3 as a critical regulator of cortical development and demonstrate that its deubiquitinase activity governs NS/PCs fate determination and brain morphogenesis through PLD1-mediated lipid signaling.

Keywords: OTUD3; brain development; neural stem/progenitor cells; deubiquitinase; PLD1; lipid metabolism; synaptic homeostasis

Introduction

Brain development is a tightly orchestrated process dependent on the precise balance of neural stem/progenitor cells (NS/PCs) proliferation, differentiation, and survival[1-3]. Deubiquitinases (DUBs) have emerged as critical regulators of developmental processes by modulating protein stability and signaling pathways[4, 5], with their ability to fine-tune protein turnover making them indispensable for maintaining the spatiotemporal precision of developmental programs[6].

OTUD3, a member of the ovarian tumor (OTU) family of DUBs, has been extensively characterized for its multifaceted roles in cellular homeostasis across diverse biological contexts. OTUD3 deubiquitinates and stabilizes PTEN to suppress PI3K-AKT signaling and tumorigenesis [7]; it specifically binds to and stabilizes p53, inhibiting its ubiquitination-mediated degradation [8]; and it acts as an energy sensor, translocating to the nucleus to deubiquitinate transcription factors such as PPARδ [9]. It also regulates pathological processes such as esophageal cancer lymph node metastasis, where nicotine-induced OTUD3 downregulation reduces ZFP36, upregulates VEGF-C mRNA, and promotes lymphangiogenesis[10]. Our previous work identified OTUD3 as a deubiquitinase for iron regulatory protein 2 (IRP2) and Fortilin in the nervous system, maintaining brain iron homeostasis and protecting dopaminergic neurons in Parkinson's disease[11, 12]. These findings establish OTUD3 as a neuroprotective factor, yet its function in mammalian brain development - particularly its regulation of NS/PCs dynamics - remains unexplored.

The developing brain requires precise regulation of protein stability at distinct stages[13]. Early neurogenesis depends on tight control of cell cycle regulators, whereas post-mitotic neuronal maturation requires coordinated synaptic protein homeostasis[14, 15]. We hypothesized that OTUD3 may regulate brain development through stage-specific substrate stabilization, coordinating the transition from proliferative to differentiated states.

To test this hypothesis, we combined *in vivo* genetic models, *in vitro* NS/PCs

assays, and quantitative proteomics to investigate OTUD3 function in mouse brain development. Our results reveal that OTUD3 acts as a stage-specific regulator: it controls early NS/PCs proliferation through established substrates and governs post-differentiation neuronal maturation through phospholipase D1 (PLD1)-mediated lipid signaling.

Materials and methods

Experimental animals

Otud3$^{-/-}$ mice and *Otud3*^{TG} mice were kindly provided by Professor Lingqiang Zhang (State Key Laboratory of Proteomics, National Center of Protein Sciences (Beijing, China), Beijing Institute of Lifeomics, Beijing, China). All mice were housed in a specific pathogen-free (SPF) animal facility under controlled conditions (22–25 ℃, 12 h light/dark cycle) with free access to food and water. All animal experiments were approved by the Ethical Committee of Laboratory Animals of Qingdao University.

Genomic DNA was extracted from mouse tail tips using the phenol-chloroform method. PCR amplification of the *Otud3* gene locus was performed with specific primers for WT, *Otud3*$^{-/-}$ and *Otud3*^{TG} mice. PCR products were separated by 1.5% agarose gel electrophoresis, and genotypes were determined by the size of the amplified fragments.

Brains were harvested from *Otud3*$^{-/-}$, *Otud3*^{TG}, and WT mice at E14-15, postnatal day 1 (D1), 1 month (1 M), and adult stages. Brain volume was quantified using ImageJ software. For histological staining and immunofluorescence staining, brain tissues were fixed in 4% paraformaldehyde (PFA) overnight at 4℃ and then cryoprotected in 30% sucrose, and sectioned at 20 μm thickness.

Novel object recognition test

The novel object recognition test was performed in a sound-attenuated room (50 lux, < 40 dB background noise) using a 50 cm × 50 cm × 50 cm gray open-field arena. The procedure consisted of three phases over three consecutive days: habituation, familiarization, and testing. Habituation (Day 1): Mice were placed individually into the empty arena to explore freely for 10 min. Familiarization (Day 2): Two identical

objects were placed 5 cm away from the walls. Mice were allowed to explore the objects for 10 min. Testing (Day 3): Twenty-four hours later, one identical object was replaced with a novel object (randomized left/right placement). Mice were reintroduced to the arena for a 10 min test session. The apparatus and objects were cleaned with 75% ethanol between trials to eliminate olfactory cues. Exploration was defined as directing the nose toward the object at a distance of < 2 cm or touching it; sitting on or climbing the object was excluded. Parameter analysis, including total distance traveled, was performed using the Smart 2.0 tracking and analysis system.

Fear conditioning task

The fear conditioning paradigm comprised three phases (habituation, conditioning, and testing) separated by 24 h. On day 1, mice explored the chamber for 10 min without stimulation; the apparatus was cleaned with 75% ethanol between subjects. On day 2, following a 5-min baseline, mice received five CS-US pairings (CS: 20 s, 90 dB tone; US: 2 s, 0.3 mA footshock, co-terminating with CS), with a 2-min inter-trial interval. Mice remained in the chamber for 1 min after the last trial. On day 3, contextual fear was assessed by returning mice to the original chamber for 5 min (300 s) without stimulation. One hour later, cued fear was tested in a modified context (altered floor, wall color, and odor), consisting of a 4-min baseline followed by four CS presentations (20 s each) with 60-s inter-stimulus intervals. Freezing (immobility >1 s, excluding respiration) was quantified automatically using the PanLab FreezeScan system and confirmed manually by two blinded investigators. Freezing percentage was calculated as the proportion of freezing time during the total valid duration (300 s for contextual test; 80 s for CS periods in cued test).

Human dataset analysis

Publicly available transcriptomic datasets of human brain tissues were retrieved from UCSC Cell Browser (https://cells.ucsc.edu/?ds=autism&gene=ENSG00000169914). Differential expression level of OTUD3 in cortex was analyzed based on the published datasets.

OTUD3 expression in human dopaminergic neurons from normal brains, lewy body dementia (LBD) and Parkinson's disease cases was retrieved from Slide-seq data

[16] in Single Cell PORTAL (https://singlecell.broadinstitute.org/).

Nissl staining

Nissl staining was performed with cresyl violet solution kit (Beyotime Biotechnology, CN). Brain tissue sections were washed three times with 0.01 M PBS for 5 min each to remove the OCT embedding medium, followed by uniform coverage with cresyl violet staining solution and incubation at room temperature for 10 min; the sections were then sequentially immersed in 75%, 90%, and 100% ethanol for 4 min each, subsequently treated with xylene twice for 4 min per wash, and finally mounted with neutral mounting medium for storage, with the staining results captured and saved using an Olympus microscope. Brain sections were imaged under a light microscope.

Isolation and culture of NS/PCs

NS/PCs were isolated from the cerebral cortices of E14-15 *Otud3*$^{-/-}$ and WT mouse embryos. Cortical tissues were mechanically dissociated into single-cell suspensions and cultured in neurosphere medium consisting of DMEM/F12 (1:1) supplemented with 20 ng/mL epidermal growth factor (EGF), 10 ng/mL basic fibroblast growth factor (bFGF), N2 (1:100), B27 (1:50), 100 U/mL penicillin, 100 μg/mL streptomycin (all from Gibco, US) and 2.5 μg/mL heparin (Sigma-Aldrich, US) at 37℃ in a 5% CO_2 incubator. Neurospheres were passaged every 5 days, and NS/PCs on passage number 2 to 3 were used for following experiment. Upon the passage, spheres were trypsinized and mechanically triturated into single-cell suspensions and replated at 1×10^5 cells/mL either in growth medium or differentiation medium (contained DMEM/F12 with 1% fetal bovine serum (FBS; Invitrogen, US), 1% N2, and 2% B27 supplement, 100 U/mL penicillin, 100 μg/mL streptomycin).

Functional assays of NS/PCs *in vitro*

Neurosphere formation assay: NS/PCs from *Otud3*$^{-/-}$ and WT mice were seeded at a density of 1×10^3 cells/well in 24-well plates. After 4 days of culture, the number and diameter of neurospheres were counted and measured under a light microscope. Three independent experiments were performed, with five replicate wells per group in each experiment.

Proliferation assay: Immunofluorescence was performed using anti-Ki67 (1:300,

Millipore) and anti-Nestin (1:200, Millipore) antibodies, with DAPI (1:1000; Roche) for nuclear counterstaining. For cell cycle analysis, NS/PCs were fixed in 70% ethanol, stained with propidium iodide (PI, 1:2000; Roche), and analyzed by flow cytometry.

Apoptosis assay: NS/PCs were harvested and stained with Annexin V-FITC and PI according to the manufacturer's instructions (FITC-Annexin V kit, BD biosciences). Apoptotic cells (Annexin V^+/PI^- and Annexin V^+/PI^+) were detected by flow cytometry, and the apoptosis rate was calculated.

Differentiation assay: NS/PCs were cultured in differentiation medium (DMEM/F12 with 1% FBS) for 7 days. Cells were then immunostained with primary antibodies against β-tubulin III (1:200, Cat# MAB360, Millipore, US), MAP2 (1:200, Cat# 4542S, CST, US), and GFAP (1:1000, Cat# MAB5564, Millipore, US). After three 5-min PBS washes, cells were incubated with FITC- or rhodamine-conjugated secondary antibodies (1:500; Life Technologies, US) for 2 h at RT, followed by three additional PBS washes and DAPI nuclear staining for 5 min. Images were captured using a fluorescence microscope (Olympus) equipped with a digital camera and OlyVIA software.

Proliferation analysis of NS/PCs *in vivo*

Brain from E14-15 *Otud3*^{TG}, and WT mouse embryos were dissected, fixed in 4% PFA, cryoprotected in 30% sucrose, and sectioned at 20 μm thickness. Immunofluorescence staining was performed with anti-Ki67 and anti-Nestin antibodies, followed by DAPI staining. The number of $Ki67^+$ and $Nestin^+$ cells in the ventricular/subventricular zone (VZ/SVZ) of the cerebral cortex was counted under a fluorescence microscope, and the density of proliferating NS/PCs was calculated.

HEK293T and SH-SY5Y Cell culture, transfection

In vitro assays were performed in HEK293T and SH-SY5Y cell line acquired from the National Collection of Authenticated Cell Cultures (Shanghai, CN). Cells were cultivated in the DMEM/F12 (Cat# SH30022.01, Hyclone, US) interpolated into 10% fetal bovine serum (Cat# FS401-02, Transerum, Beijing, CN) and 1% penicillin/streptomycin (Cat# P1400, Solarbio, CN) in a 37℃, 5% CO_2 incubator.

Full-length OTUD3-WT, PLD1, and C76A mutant were cloned into pCMV-Myc

vectors as specified. Flag-tagged plasmids including Flag-OTUD3, Flag-PLD1, Flag-OTU, Flag-UBA, Flag-UBA+Tail and Flag-Tail were generated in the pCMV-Flag backbone and purchased from OBIO Technology. Lentiviruses carrying shRNA targeting human *OTUD3* (Target sequence: GGACAATAACAGAAGCGAA) was from OBIO (Shanghai, China). The plasmids were transfected into cells with lipofectamine 3000 reagent (Invitrogen, Cat# L3000015, USA) according to the specification.

Quantitative real-time polymerase chain reaction (qRT-PCR).

Total RNA was extracted using TRIzol reagent (Cat# R701-02, Invitrogen, US) according to the manufacturer's instructions. 1μg RNA was reverse-transcribed into cDNA using HiScript III RT SuperMix for qPCR (Vazyme, Cat# R323-01). qPCR was performed with ChamQ Universal SYBR qPCR Master Mix (Vazyme, Cat# Q711-02) to quantify PLD1 and GAPDH transcript levels. The primer sequences are as follows: homo-PLD1-f: TGCTGGGAAAGCGTGACAGT, homo-PLD1-r: AGCCAAGGACAACCCTAAAGCA; GAPDH-f: CCAAGGTCATCCATGACAACTT, GAPDH-r: AGGGGCCATCCACAGTCTT. Relative mRNA levels were evaluated by the $2^{-\Delta\Delta CT}$ formula and results were performed as the fold-change of control samples.

Western blotting and Immunoprecipitation

Cells were lysed in RIPA buffer (CWBio), and lysates were cleared by centrifugation at 12,000 rpm for 10 min at 4°C. Immunoprecipitations were performed using the indicated primary antibody and protein A/G agarose beads (Santa Cruz, US) at 4°C. The immunocomplexes were then washed with HEPES lysis buffer five times. Proteins were resolved by 10% SDS-PAGE, transferred to PVDF membranes (Millipore), blocked with 5% nonfat milk in TBST for 1 h at RT, and incubated with primary antibodies overnight at 4°C, followed by HRP-conjugated secondary antibodies for 2 h at RT. Primary antibodies used: mouse anti-β-tubulin III (1:1000, Cat#MAB360, Millipore, US), mouse anti-MAP2 (1:1000, Cat#4542S, CST, US), mouse anti-GFAP (1:1000; Cat#MAB5564, Millipore, US), rabbit anti-OTUD3

(1:1000, Cat# 29622-1-AP, Proteintech, US), rabbit anti-PLD1 (1:1000, Cat# 18355-1-AP, Proteintech, US) , mouse anti-PLD1 (1:1000, Cat# sc-28314 Santa Cruz, CA, US), mouse anti-Flag (1:1000, Cat# M185-3L, MBL, JP), mouse anti-Myc (1:1000, Cat# M192-3, MBL, JP), mouse anti-Ub (1:1000, Cat# 3936S, CST, US), rabbit anti-SYB (1:1000, Cat# abs146452, Absin, CN), and rabbit anti-GAPDH (1:10,000; Cat# A19056, Abclonal, CN). The following secondary antibodies were used for Western blotting analysis: anti-rabbit IgG-HRP (1:10,000, Cat# 39572S) and anti-mouse IgG-HRP (1:10,000, Cat# 56090S), both from CST. Blots were developed with ECL substrate (Millipore), and band intensities were quantified using ImageJ (v1.61).

Protein half-life assay

For the PLD1 half-life assay, Lipofectamine 3000 transfection was performed when HEK293T cells in 2 cm plates reached about 60% confluence. Plasmids were used in transfection as indicated in individual experiments. Twenty-four hours after transfection, cells were treated with 100 μg/mL cycloheximide (CHX, MedChem Express, Cat# HY-12320, US) for the indicated durations (2, 4, 6, and 10 h) prior to collection.

Ubiquitin Conjugation Assay

Cells were treated with 20 μM MG132 (proteasome inhibitor, Calbiochem) for 8 h prior to collection. After washing with PBS, cells were pelleted and lysed in HEPES buffer containing 1% DTT and 1× protease inhibitor cocktail. Lysates were centrifuged, and the supernatants were incubated with anti-Flag or anti-Myc antibodies for 5 h, followed by protein A/G agarose beads for an additional 8 h at 4°C. Beads were washed five times with HEPES buffer, and bound proteins were eluted by boiling in SDS-PAGE sample buffer for immunoblotting with anti-ubiquitin antibody.

Enzyme-linked immunosorbent assay (ELISA)

Phosphatidic Acid (PA) was assayed by corresponding ELISA kits (Fantaibio, Cat# FT-P33125R, CN). The signal at a wavelength of 450 nm by a multimode plate reader was measured. The concentrations were calculated by drawing a standard curve.

Confocal Microscopy

For immunofluorescence analysis of subcellular localization, cells were fixed with

4% paraformaldehyde, permeabilized with 0.3% Triton X-100 in PBS, and incubated with anti-PLD1 and anti-OTUD3 antibodies overnight at 4℃, followed by FITC- or rhodamine-conjugated secondary antibodies (1:500, Cat# A21202, Cat# A31572, Life Technologies, US) for 2 h at RT. Nuclei were stained with DAPI, and images were acquired using an inverted confocal microscopy (Leica, STELLARIS 5).

Proteomic profiling and bioinformatics analyses

Brain tissues from E14-15 and D1 *Otud3*$^{-/-}$ and WT mice were harvested, and total protein was extracted using RIPA buffer supplemented with a protease inhibitor cocktail. Protein concentration was determined using the BCA assay. The quality of extracted protein was verified by SDS-PAGE. For proteomic analysis, 4D mass spectrometry-based proteomics was applied, combining liquid chromatography-tandem mass spectrometry (LC–MS/MS). The workflow included two MS acquisition modes: 4D-DDA (data-dependent acquisition) and 4D-DIA (data-independent acquisition). Data independent acquisition (DIA) was performed for quantitative proteomic analysis. Raw mass spectrometry data were processed using MaxQuant software, and differentially expressed proteins were identified with the criteria of Foldchange > 1.5 and adjusted $P < 0.05$.

Kyoto Encyclopedia of Genes and Genomes (KEGG) pathway enrichment analysis and Gene Ontology (GO) functional enrichment analysis of differentially expressed proteins (DEPs) were performed using the clusterProfiler R package. GO analysis included three ontologies: biological process (BP), cellular component (CC), and molecular function (MF). The top 20 enriched KEGG pathways and 30 enriched GO terms were visualized, and statistical significance was determined by the adjusted *P* value (FDR) < 0.05.

Statistical Analysis

All experimental data are presented as the mean ± standard deviation (SD) from at least three independent experiments. Statistical analysis was performed using GraphPad Prism 10 software. Comparisons between two groups were conducted using the unpaired Student's t-test, and comparisons among multiple groups were performed

using one-way analysis of variance (ANOVA) followed by Tukey's post-hoc test. $P < 0.05$ was considered statistically significant.

Results

1. OTUD3 is ubiquitously expressed in the developing mouse brain and aberrantly expressed in human NDDs

To investigate the expression pattern of OTUD3 in the developing brain, we analyzed single-cell RNA-seq data from cortex. t-SNE analysis showed that OTUD3 is specifically enriched in excitatory cortical neurons (L2/3, L4, L5/6-CC), inhibitory interneurons (PV, SST, SV2C, VIP), and maturing neurons, with near-absence in glia, endothelium, and $NRGN^{+}$ neurons (Fig. 1A). This neuron-specific expression pattern suggests that OTUD3 primarily functions in neuronal lineages during brain development.

Analysis of public human datasets revealed graded OTUD3 expression in dopaminergic neurons: highest in normal brains, moderate in Lewy body dementia, and lowest in Parkinson's disease (Fig. 1B), suggesting conserved roles in neuronal development and neurodegeneration.

To assess the functional consequences of OTUD3 loss, we generated OTUD3 knockout (*Otud3*$^{-/-}$) mice. Behavioral tests identified severe recognition memory deficits: *Otud3*$^{-/-}$ mice displayed consistently reduced recognition indices at 1, 3, and 6 months of age in the novel object recognition test (Fig. 1C, D), indicative of impaired recognition memory. Additionally, *Otud3*$^{-/-}$ mice exhibited decreased freezing time in fear conditioning assays (Fig. 1E, F), suggesting defective fear memory formation.

Morphologically, OTUD3 deficiency caused profound developmental brain abnormalities. Gross anatomical observation and quantitative measurement verified reduced brain size, length and width in *Otud3*$^{-/-}$ mice across E14-15, D1, and 1-month stages (Fig. 1G-I). Histological staining further validated thinner cerebral cortices and decreased cortical cellular density from embryonic to postnatal stages (Fig. 1J, K). Notably, *Otud3*^{TG} mice recapitulated the reduced brain volume phenotype of *Otud3*$^{-/-}$ mice (Fig. S1A, S1B), indicating that aberrant elevation of OTUD3 is similarly

detrimental to brain morphogenesis. These data establish that OTUD3 is essential for normal brain morphogenesis and cognitive function.

2. OTUD3 cell-autonomously regulates NS/PCs proliferation, apoptosis, and differentiation

To assess cell-autonomous OTUD3 effects, NS/PCs were isolated from E14-15 cortex of WT and *Otud3*$^{-/-}$ and *Otud3*^{TG} mice. Neurosphere assays showed that *OTUD3*$^{-/-}$ NS/PCs formed more and larger neurospheres than WT controls (Fig. 2A, 2B), indicating enhanced proliferation. This was also supported by increased Ki67^{+} cells in *Otud3*$^{-/-}$ cultures (Fig. 2D, 2E). Cell cycle analysis further revealed elevated S and G2/M fractions and reduced G1 phase in *Otud3*$^{-/-}$ NS/PCs (Fig. 2F-I), demonstrating accelerated cell cycle progression. Conversely, *Otud3*^{TG} NS/PCs impaired neurosphere formation and decreased Ki67^{+} cell ratios (Fig. S1C-I), confirming OTUD3 as a negative regulator of NS/PCs proliferation. Additionally, OTUD3 deficiency reduced NS/PCs apoptosis relative to WT controls (Fig. 2J, 2K), demonstrating an anti-apoptotic role of OTUD3 ablation in maintaining the NS/PCs pool. For NS/PCs differentiation, immunofluorescence staining showed that *Otud3*$^{-/-}$ cultures contained more β-tubulin III^{+} immature neurons and MAP2^{+} mature neurons than WT groups, with unchanged GFAP^{+} astrocyte proportions (Fig. 2L-S). Western blotting results further supported these alterations (Fig. 2R-U). Consistent with this, OTUD3 overexpression showed no significant changes in neuronal or astrocytic differentiation (Fig. S1J-L, S1N-O). These data establish that OTUD3 cell-autonomously restrains premature neuronal differentiation while leaving astrocytic lineage commitment unaffected, thereby preserving the temporal order of neurogenesis.

These findings indicate that both insufficient and excessive OTUD3 disrupt normal brain development, albeit through distinct cellular mechanisms. While loss promotes proliferation and premature differentiation, gain primarily impairs proliferative capacity. This finding underscores that precise regulation of OTUD3 expression - not merely its presence - is essential for maintaining the delicate balance of cortical development.

3. Stage-specific proteomic remodeling in the OTUD3-deficient developing brain

To investigate OTUD3's role in cortical development, 4D label-free proteomics was performed on WT and *Otud3*$^{-/-}$ cortices at E14-15 and D1, with validated reproducibility (Fig. S2A-C). Principal component analysis (PCA) and clustering revealed genotype-dependent proteomic divergence (Fig. S2E-J). Pairwise correlation showed strong intra-group but weak inter-group correlations at both stages (Fig. S3A, S3B), and OTUD3 loss disrupted the developmental proteomic trajectory between E14-15 and D1 (Fig. S3C, S3D). Thus, OTUD3 genotype and developmental stage are key determinants of cortical proteomic profiles, with *Otud3* KO driving significant divergence at both stages.

Quantification of DEPs showed 90 upregulated and 134 downregulated proteins at E14-15, and 78 upregulated and 174 downregulated proteins at D1 (Fig. S4A-C, Table1). Venn diagram analysis (Fig. S4D) identified both shared and unique DEPs between E14-15 and D1, suggesting that OTUD3 deficiency induces both early-onset and progressive molecular dysregulation during brain development. Hierarchical clustering of DEPs (Fig. 3A, 3B) demonstrated distinct expression patterns in *Otud3*$^{-/-}$ mice compared to WT controls, with stage-specific clusters of up- and downregulated proteins.

KEGG pathway enrichment analysis revealed distinct stage-specific signatures (Fig. 3C-H, S4E-F). At E14-15, DEPs were significantly enriched in cell cycle, DNA replication, and p53 signaling (Fig. 3C), consistent with the enhanced proliferation observed in *Otud3*$^{-/-}$ NS/PCs. At P1, the enrichment pattern shifted markedly toward cellular senescence, ferroptosis, HIF-1 signaling, and lipid metabolism (Fig. 3F), suggesting that metabolic homeostasis remains disrupted after differentiation.

GO enrichment analysis validated this stage transition (Fig.3I-N, S4G-H). At E14-15, up-regulated genes were enriched in DNA replication, cell division and mitotic nuclear division, whereas down-regulated genes were associated with immune response, inflammatory response and cell adhesion (Fig.3I-K). At D1, up-regulated genes remained enriched in mitotic cell cycle and chromosome organization, while

down-regulated genes were involved in oxidation-reduction, cholesterol metabolism and lipid biosynthesis (Fig.3L-N). Notably, lipid metabolic, fatty acid metabolic, and lipid biosynthetic processes ranked among the top-enriched biological processes at both developmental stages, with particularly strong enrichment observed for downregulated genes at D1.

4. OTUD3 Deficiency Alters PLD1-Related Pathways

Hierarchical clustering heatmap was generated for proteins that were downregulated in both KO-E14-15 and KO-D1 stages, to verify their consistent reduction across these two developmental time points (Figure 4A). To further characterize proteins persistently downregulated in both KO-E14-15 and KO-D1 groups, KEGG pathway enrichment analysis was performed, which identified significant enrichment in lipid metabolism-related pathways including ether lipid metabolism and sphingolipid signaling pathway (Figure 4B). Its location within the perturbed lipid - metabolic network at D1 guided our subsequent mechanistic investigations. Subsequent PPI network analysis identified PLD1 as the top hub protein with the highest node degree, which was significantly downregulated upon *Otud3* knockout. (Figure 4C). PLD1 (Q9Z280) was identified as the core hub gene with the highest connectivity degree in this network, and it was markedly downregulated in the KO-D1 group. As a central enzyme in lipid metabolism, PLD1 participates in phospholipid hydrolysis and lipid second-messenger generation. Together, these results indicate that *Otud3* knockout leads to reduced PLD1 abundance, which may contribute to the global suppression of lipid metabolism pathways at both developmental stages.

5. OTUD3 stabilizes PLD1 through forming a complex and deubiquitination

The persistent downregulation of PLD1 across developmental stages, combined with the late-stage lipid metabolic suppression, prompted us to investigate whether PLD1 is a direct substrate of OTUD3. Published studies demonstrate that *Pld1* knockout mice exhibit reduced brain volume, aberrant neuronal differentiation, and cognitive impairments [17] - phenotypes highly consistent with our *Otud3*$^{-/-}$ data and

further supporting PLD1 as a mechanistic candidate.

We next examined whether OTUD3 directly modulates PLD1 protein stability. shRNA-mediated knockdown of OTUD3 significantly reduced PLD1 protein levels, whereas ectopic expression of OTUD3 elevated PLD1 protein in a dose-dependent manner (Fig. 5A-H). Notably, the catalytically inactive OTUD3^{C76A} mutant failed to alter PLD1 levels, indicating that OTUD3 stabilization of PLD1 requires its deubiquitinase activity (Fig. 5I-J). Proteasome inhibition with MG132 rescued PLD1 reduction caused by OTUD3 knockdown, while Myc-OTUD3 overexpression increased PLD1 abundance (Fig. 5K-N); and cycloheximide chase assays revealed that OTUD3 significantly extended PLD1 half-life (Fig. 5O-R). Immunofluorescence confirmed subcellular colocalization of OTUD3 and PLD1 (Fig. 5S), and reciprocal co-immunoprecipitation demonstrated their direct interaction (Fig. 5T). Furthermore, OTUD3 overexpression markedly reduced PLD1 polyubiquitination (Fig. 5U), and domain mapping identified the OTU catalytic domain as essential for PLD1 binding (Fig. 5V). Together, these data establish that OTUD3 interacts with PLD1 via its OTU domain and stabilizes it through deubiquitination, preventing proteasomal degradation.

6. The OTUD3–PLD1 axis maintains lipid–synaptic signaling

To determine whether PLD1 functionally mediates OTUD3-dependent effects, we performed rescue experiments using SH-SY5Y cell line. Ectopic expression of Flag-PLD1 restored PLD1 protein levels in *OTUD3*-knockdown cells (Fig. 6A-C) and rescued PLD enzymatic activity, as measured by phosphatidic acid (PA) production (Fig. 6D). Moreover, PLD1 overexpression reversed the reduction of SYP, a presynaptic marker, caused by OTUD3 depletion (Fig. 6E, F).

These findings establish that OTUD3 stabilizes PLD1 to maintain lipid enzymatic activity and synaptic protein homeostasis. Given that PLD1-derived PA governs neurite outgrowth and presynaptic development, the OTUD3-PLD1 axis provides a molecular basis for the synaptic and cognitive deficits observed in *Otud3*$^{-/-}$ mice.

Discussion

Our findings reveal that OTUD3 functions as a stage-specific developmental regulator. At early embryonic stages (E14-15), OTUD3 controls NS/PCs proliferation and survival, likely through its established substrates PTEN and p53[7, 8]. Quantitative proteomics confirmed that OTUD3 deficiency disrupts cell cycle and DNA replication pathways at this stage. At post-differentiation stages (D1), the regulatory focus shifts to lipid metabolism and synaptic signaling, mediated by the newly identified OTUD3-PLD1 axis. This stage-specific substrate switching from cell cycle regulators to lipid enzymes, enables OTUD3 to coordinate sequential developmental programs, ensuring proper transition from proliferative to differentiated states.

We demonstrate that OTUD3 physically interacts with PLD1 via its OTU catalytic domain, removes ubiquitin chains, and extends PLD1 protein half-life. This deubiquitination mechanism preserves PLD1 enzymatic activity and maintains synaptic protein homeostasis, as evidenced by PLD1-mediated rescue of synaptophysin levels. OTUD3 and PLD1 knockout mice share overlapping phenotypes of reduced brain volume, cognitive impairment, and aberrant neuronal differentiation, offering robust genetic evidence for this molecular axis[17]. Unlike PTEN and p53, which primarily control cell cycle arrest, PLD1 specifically drives post-mitotic neuronal maturation through phosphatidic acid-mediated membrane trafficking and synaptic morphogenesis. The OTUD3-PLD1 axis therefore fills a critical mechanistic gap, explaining why OTUD3 deficiency causes cortical hypoplasia beyond simply enhanced proliferation.

OTUD3 exhibits graded expression in human dopaminergic neurons, with the highest levels in normal brains, moderate levels in Lewy body dementia, and the lowest levels in Parkinson’s disease, implying its potential relevance to brain function and neurodegenerative disease pathogenesis. Both OTUD3 knockout and overexpression resulted in abnormal brain volume, indicating that precise control of OTUD3 expression is essential for normal development. However, we caution against interpreting this as classical "dosage sensitivity" in the haploinsufficiency sense. Rather, our data suggests that OTUD3 must be maintained within an optimal expression range: insufficient OTUD3 fails to stabilize critical substrates (PLD1, PTEN and p53), whereas excessive OTUD3 may hyper-stabilize targets or sequester interacting partners,

disrupting normal protein turnover dynamics. *Otud3*$^{-/-}$ mice undergo accelerated cell cycle progression and premature neuronal differentiation, whereas OTUD3 overexpression hinders neural progenitor proliferation; these disparate cellular mechanisms corroborate this interpretation.

The *in vitro-in vivo* discrepancy further highlights the complexity of OTUD3 regulation. While OTUD3 deficiency enhanced NS/PCs proliferation in culture, both *Otud3*$^{-/-}$ and *Otud3*^{TG} mice showed reduced brain size *in vivo*. This paradoxical convergence of phenotypes—where both loss-of-function and gain-of-function impair brain development — exemplifies the "Goldilocks effect" in neurodevelopment, suggesting that OTUD3 expression must be maintained within a precise window to ensure normal cortical morphogenesis. This divergence likely reflects non-cell-autonomous compensation within the intact brain microenvironment, where cell-cell interactions and systemic signals buffer cell-autonomous effects[18-21]. Our findings thus underscore the necessity of validating *in vitro* observations in intact organisms, and reveal that precise regulation of OTUD3 dosage is critical for neural stem cell fate determination and brain homeostasis.

4D label-free proteomics reveals that OTUD3 deficiency triggers stage-specific proteomic remodeling in the developing cerebral cortex. Loss of OTUD3 disrupts the normal developmental proteomic trajectory, with embryonic changes enriched in cell-cycle pathways and postnatal alterations converging on cellular senescence, ferroptosis, and lipid metabolism. Notably, lipid metabolic processes are suppressed at both developmental stages. Analysis of persistently downregulated proteins highlights enrichment in lipid metabolism pathways, and PPI network analysis nominates PLD1 as the core hub of this network. As a central lipid-metabolizing enzyme, reduced PLD1 abundance likely drives global lipid metabolic suppression in the OTUD3-deficient cortex, bridging OTUD3 deletion to disrupted neuronal and synaptic phenotypes. Given that PLD1 and lipid signaling are increasingly implicated in synaptic dysfunction and neurodegeneration, dysregulation of the OTUD3-PLD1 axis may represent a shared pathological mechanism linking developmental perturbations to late-onset neuronal vulnerability [22, 23].

Mechanistically, we identify PLD1 as a direct substrate of OTUD3. OTUD3 binds PLD1 via its OTU catalytic domain and stabilizes PLD1 through deubiquitination, thereby protecting PLD1 from proteasomal degradation. Loss of OTUD3 decreases PLD1 protein abundance, whereas OTUD3 overexpression elevates PLD1 levels in a dose-dependent manner; this stabilization relies on the deubiquitinase activity of OTUD3. Functionally, consistent with previous reports, *Pld1* knockout mice display brain volume reduction, defective neuronal differentiation, and cognitive deficits [17, 24], phenotypes recapitulated in our *Otud3*$^{-/-}$ model. Collectively, these observations support a model in which PLD1 acts as a key downstream effector mediating OTUD3 functions in the brain, and suggest that developmental dysregulation of the OTUD3-PLD1 axis may predispose to late-onset neurological deficits.

The OTUD3-PLD1 axis sustains lipid-synaptic signaling. Rescue experiments in SH-SY5Y cells show that reintroduction of PLD1 restores PLD1 protein abundance and its enzymatic activity to produce phosphatidic acid in OTUD3-deficient cells. PLD1 overexpression also reverses the decreased level of presynaptic marker SYP triggered by OTUD3 depletion. Collectively, OTUD3 maintains lipid metabolism and presynaptic signaling through stabilizing PLD1. Thus, disruption of the OTUD3-PLD1 pathway may contribute to the neuronal and synaptic defects observed in *Otud3*$^{-/-}$ mice.

Several limitations remain. Our PLD1 deubiquitination and rescue experiments were performed in cell lines; primary NS/PCs and *in vivo* rescue assays are needed to validate the OTUD3-PLD1 axis under physiological neurogenesis conditions. Future work will utilize Nestin-Cre conditional *Otud3* knockout mice and human iPSC cortical organoids to eliminate systemic confounding effects and verify conserved human regulatory mechanisms.

In conclusion, this study identifies OTUD3 as a novel dose-sensitive regulator of mouse brain development that is specifically expressed in neurons and controls NS/PCs fate cell-autonomously. OTUD3 deficiency triggers stage-specific proteomic remodeling, impairs global protein regulation, disrupts coordinated developmental pathways, and ultimately causes abnormal brain development and cognitive

dysfunction. These findings expand the known functions of OTUD3 into neurodevelopment and provide a potential molecular target for understanding and treating NDDs associated with abnormal brain development. [11, 12]

Contributions

H.J. and Q.J. conceived the project and designed experiments. T.X. performed the proteomic analysis and *in vitro* experiments with *Otud3*$^{-/-}$ mice. Q.Z. conducted the *in vitro* experiments using *Otud3*^{TG} mice. K.R., Y.L. and S.L. carried out brain tissue collection, Nissl staining and behavioral tests. Y.C. conducted the biochemical validation of PLD1 as a direct OTUD3 substrate. X.H. and Z.Y. helped perform the proteomic analysis. Y.Z. and J.F. assisted with animal genotyping, breeding, and husbandry. Q.J. wrote the paper with input from all the authors.

Funding

This study was supported by the National Natural Science Foundation of China (32371013, 82471274, 82071429, 82301787), The Natural Science Foundation of Shandong Province (ZR2019ZD31, ZR2026MS1495), Taishan Scholars Program (tsqn202408166).

Data Availability Statement

All data generated or analyzed during this study are included.

Acknowledgments

We thank Lingqiang Zhang (State Key Laboratory of Proteomics, National Center of Protein Sciences (Beijing, China), Beijing Institute of Lifeomics, Beijing, China) for kindly gifting the *OTUD3*$^{-/-}$ and *OTUD3*^{TG} mice.

References

1. Rakic, P., *Evolution of the neocortex: a perspective from developmental biology.* Nat Rev Neurosci, 2009. **10**(10): p. 724-35.
2. Adams, K.V. and C.M. Morshead, *Neural stem cell heterogeneity in the mammalian forebrain.* Prog Neurobiol, 2018. **170**: p. 2-36.
3. Mattocks, M. and V. Tropepe, *Know thy neighbor: Modeling spatiotemporal cell-fate patterns in a neural stem cell niche.* Cell Stem Cell, 2021. **28**(8): p. 1339-1340.
4. Clague, M.J., S. Urbe, and D. Komander, *Breaking the chains: deubiquitylating enzyme specificity begets function.* Nat Rev Mol Cell Biol, 2019. **20**(6): p. 338-352.
5. Zhang, Z., et al., *MLKL-USP7-UBA52 signaling is indispensable for autophagy in brain*

through maintaining ubiquitin homeostasis. Autophagy, 2025. **21**(2): p. 424-446.
6. Xu, Z., et al., *Deubiquitinase Mysm1 regulates neural stem cell proliferation and differentiation by controlling Id4 expression.* Cell Death Dis, 2024. **15**(2): p. 129.
7. Yuan, L., et al., *Deubiquitylase OTUD3 regulates PTEN stability and suppresses tumorigenesis.* Nat Cell Biol, 2015. **17**(9): p. 1169-81.
8. Pu, Q., et al., *Tumor suppressor OTUD3 induces growth inhibition and apoptosis by directly deubiquitinating and stabilizing p53 in invasive breast carcinoma cells.* BMC Cancer, 2020. **20**(1): p. 583.
9. Zhou, N., et al., *Deubiquitinase OTUD3 regulates metabolism homeostasis in response to nutritional stresses.* Cell Metab, 2022. **34**(7): p. 1023-1041 e8.
10. Wang, M., et al., *Nicotine-mediated OTUD3 downregulation inhibits VEGF-C mRNA decay to promote lymphatic metastasis of human esophageal cancer.* Nat Commun, 2021. **12**(1): p. 7006.
11. Jia, F., et al., *Deubiquitylase OTUD3 prevents Parkinson's disease through stabilizing iron regulatory protein 2.* Cell Death Dis, 2022. **13**(4):418.
12. Chen, L., et al., *Deubiquitylase OTUD3 Mediates Endoplasmic Reticulum Stress through Regulating Fortilin Stability to Restrain Dopaminergic Neurons Apoptosis.* Antioxidants (Basel), 2023. **12**(4).
13. Suk, T.R. and M.W.C. Rousseaux, *The role of TDP-43 mislocalization in amyotrophic lateral sclerosis.* Mol Neurodegener, 2020. **15**(1): p. 45.
14. Oikawa, D., et al., *OTUD1 deubiquitinase regulates NF-κB- and KEAP1-mediated inflammatory responses and reactive oxygen species-associated cell death pathways.* Cell Death Dis, 2022. **13**(8): p. 694.
15. Li, H., et al., *USP8-governed GPX4 homeostasis orchestrates ferroptosis and cancer immunotherapy.* Proc Natl Acad Sci U S A, 2024. **121**(16): p. e2315541121.
16. Kamath, T., et al., *Single-cell genomic profiling of human dopamine neurons identifies a population that selectively degenerates in Parkinson's disease.* Nat Neurosci, 2022. **25**(5): p. 588-595.
17. Burkhardt, U., et al., *Impaired brain development and reduced cognitive function in phospholipase D-deficient mice.* Neurosci Lett, 2014. **572**:48-52
18. Saiz, N., B. Plusa, and A.K. Hadjantonakis, *Single cells get together: High-resolution approaches to study the dynamics of early mouse development.* Semin Cell Dev Biol, 2015. **47-48**: p. 92-100.
19. Vining, K.H. and D.J. Mooney, *Mechanical forces direct stem cell behaviour in development and regeneration.* Nat Rev Mol Cell Biol, 2017. **18**(12): p. 728-742.
20. Zhao, Q., et al., *Effects of deubiquitylases on the biological behaviors of neural stem cells.* Dev Neurobiol, 2021. **81**(6): p. 847-858.
21. Zhang, F., et al., *Cell-autonomous and non-cell-autonomous roles of NKCC1 in regulating neural stem cell quiescence in the hippocampal dentate gyrus.* Stem Cell Reports, 2023. **18**(7): p. 1468-1481.
22. Park, S.Y., et al., *Phospholipase D1 increases Bcl-2 expression during neuronal differentiation of rat neural stem cells.* Mol Neurobiol, 2015;**51**(3):1089-102.
23. Li, W.Q., et al., *PLD1 promotes dendritic spine morphogenesis via activating PKD1.* Mol Cell Neurosci, 2019 Sep:99:103394.

24. Backman, J.D., et al., *Exome sequencing and analysis of 454,787 UK Biobank participants.* Nature, 2021. **599**(7886):628-634

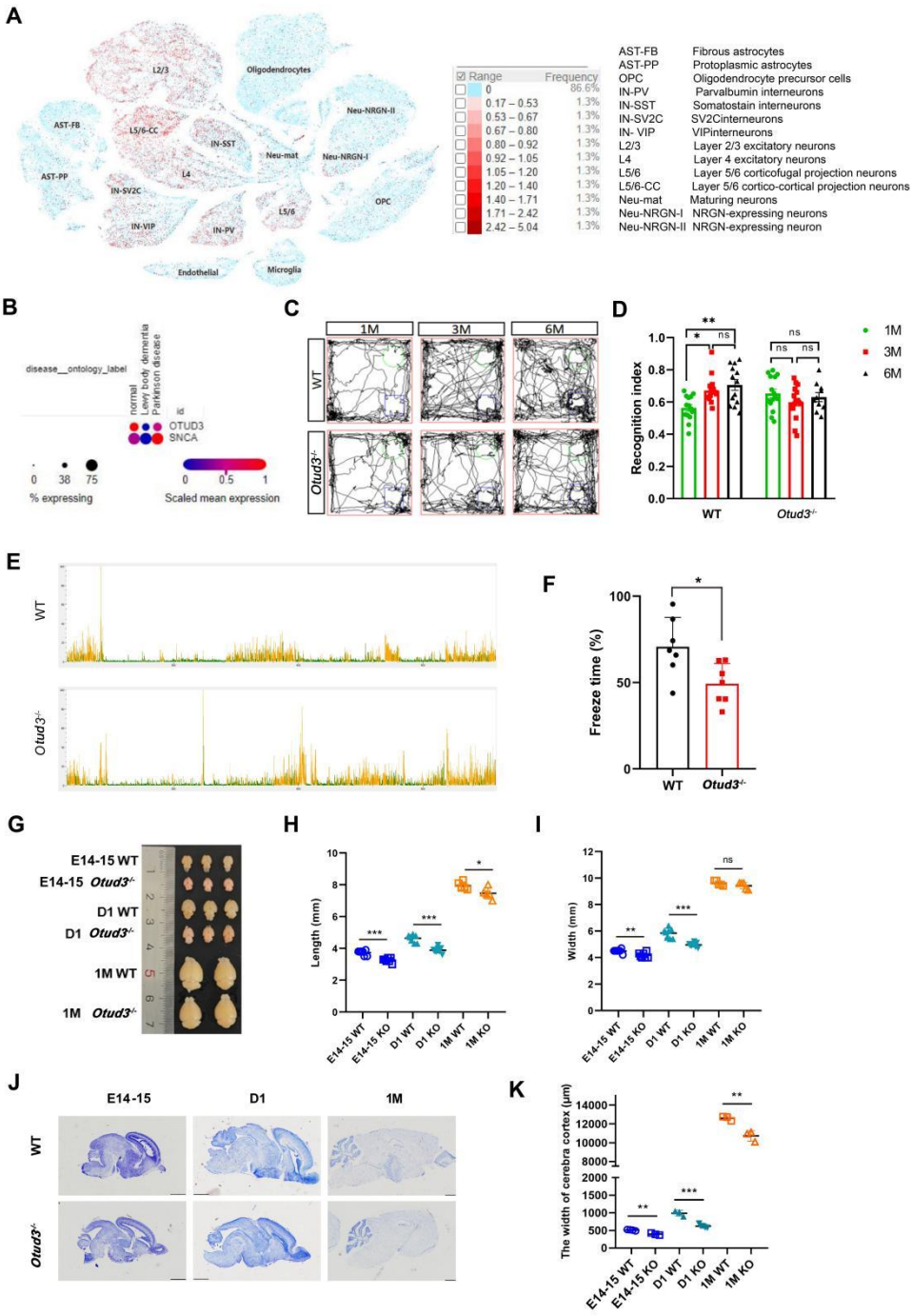


Fig. 1. OTUD3 deficiency modulates brain development and recognition/fear-related behaviors in mice. A: Cell-type-specific expression of OTUD3 in the human brain. T-distributed stochastic neighbor embedding (t-SNE) visualization of single-cell RNA sequencing data from the developing brain, colored by OTUD3 expression levels. The color scale ranges from 0 (light blue, minimal expression) to 5.04 (dark red, maximal expression). The frequency distribution of OTUD3 expression levels is shown in the inset, demonstrating that 86.6% of cells exhibit no detectable OTUD3 expression

(range 0), while the remaining cells are distributed across elevated expression bins (1.3% per bin from 0.17-5.04). **B:** Scaled mean expression and percentage of OTUD3- and SNCA-expressing cells in normal, Lewy body dementia and Parkinson's disease human brain samples. **C,D:** Representative travel trajectories of mice during the novel object recognition test (C) and quantification of the recognition index (D) in WT and *Otud3*$^{-/-}$ mice. **E,F:** Representative recordings (E) and quantitative analysis (F) of fear-related behaviors in WT and *Otud3*$^{-/-}$ mice via fear conditioning test. **G-I:** Representative whole brain images (G) and morphometric quantification of brain length and width (H-I) in WT and *Otud3* KO mice at different developmental stages. **J,K:** Representative Nissl staining of sagittal brain sections from WT and *Otud3*$^{-/-}$ mice at multiple time points (J) and quantification of cerebral cortex width (K). Data are presented as mean ± SD. ns, not significant; **P*<0.05, ***P*<0.01, ****P*<0.001.

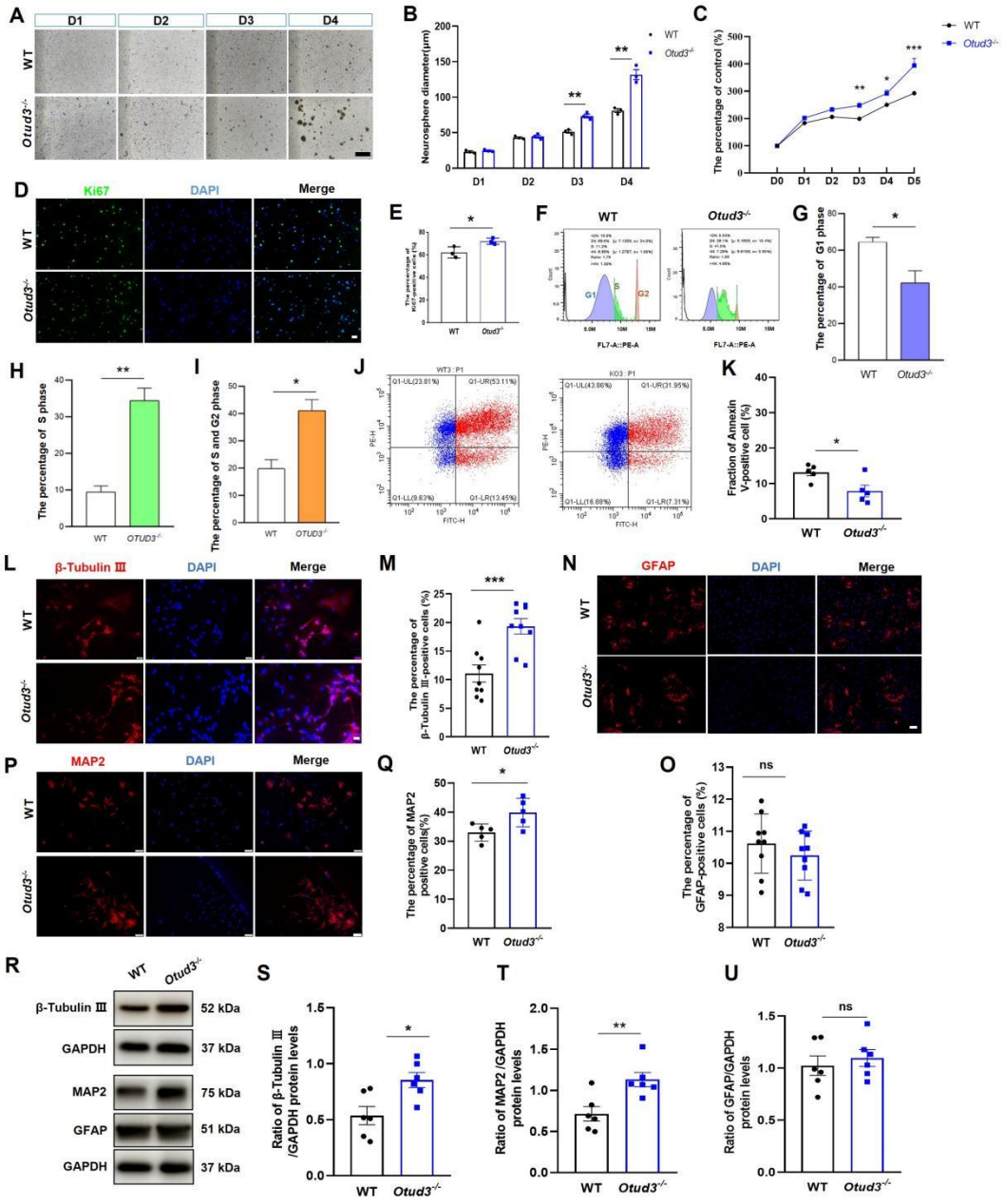


Fig. 2. OTUD3 deletion enhances NS/PCs proliferation and drives neuronal differentiation *in vitro*. A: Representative bright-field images of neurospheres from WT and *Otud3*$^{-/-}$ NS/PCs at day 1-4 (D1-D4) of culture. Scale bars=100 μm. **B,C:** Quantification of neurosphere diameter (B) and proliferation efficiency (C) in in WT and *Otud3*$^{-/-}$ NS/PCs. **D,E:** Ki67 immunofluorescence staining (D) and quantification of Ki67-positive proliferative cells in WT and *Otud3*$^{-/-}$ NS/PCs. Scale bar=100 μm. (E). **F-I:** Flow cytometric cell cycle analysis (F) and quantification of cell distribution in G1 (G), S (H) and S+G2 (I) phases in WT and *Otud3*$^{-/-}$ NS/PCs. Scale bar=100 μm.

J,K: Annexin V-FITC/PI double staining (J) and quantification of apoptotic cells (K) in WT and *Otud3*$^{-/-}$ NS/PCs. **L,M:** β-Tubulin III immunofluorescence staining (L) and quantification of β-tubulin III-positive neurons (M) in differentiated WT and *Otud3*$^{-/-}$ cells. Scale bar=20 μm. **N,O:** GFAP immunofluorescence staining (N) and quantification of GFAP-positive astrocytes (O) in differentiated WT and *Otud3*$^{-/-}$ cells. Scale bar=100 μm. **P,Q:** Map2 immunofluorescence staining (P) and quantification of Map2-positive neurons (Q) in differentiated WT and *Otud3*$^{-/-}$ cells. Scale bar=20 μm. **R-U:** Western blotting (R) and quantitative analysis of β-tubulin III (S), MAP2 (T) and GFAP (U) protein levels in differentiated cells, with GAPDH as loading control. Data are presented as mean ± SD. *$P < 0.05$, **$P < 0.01$, ***$P < 0.001$, ns, not significant vs. WT control by unpaired two-tailed Student's t-test.

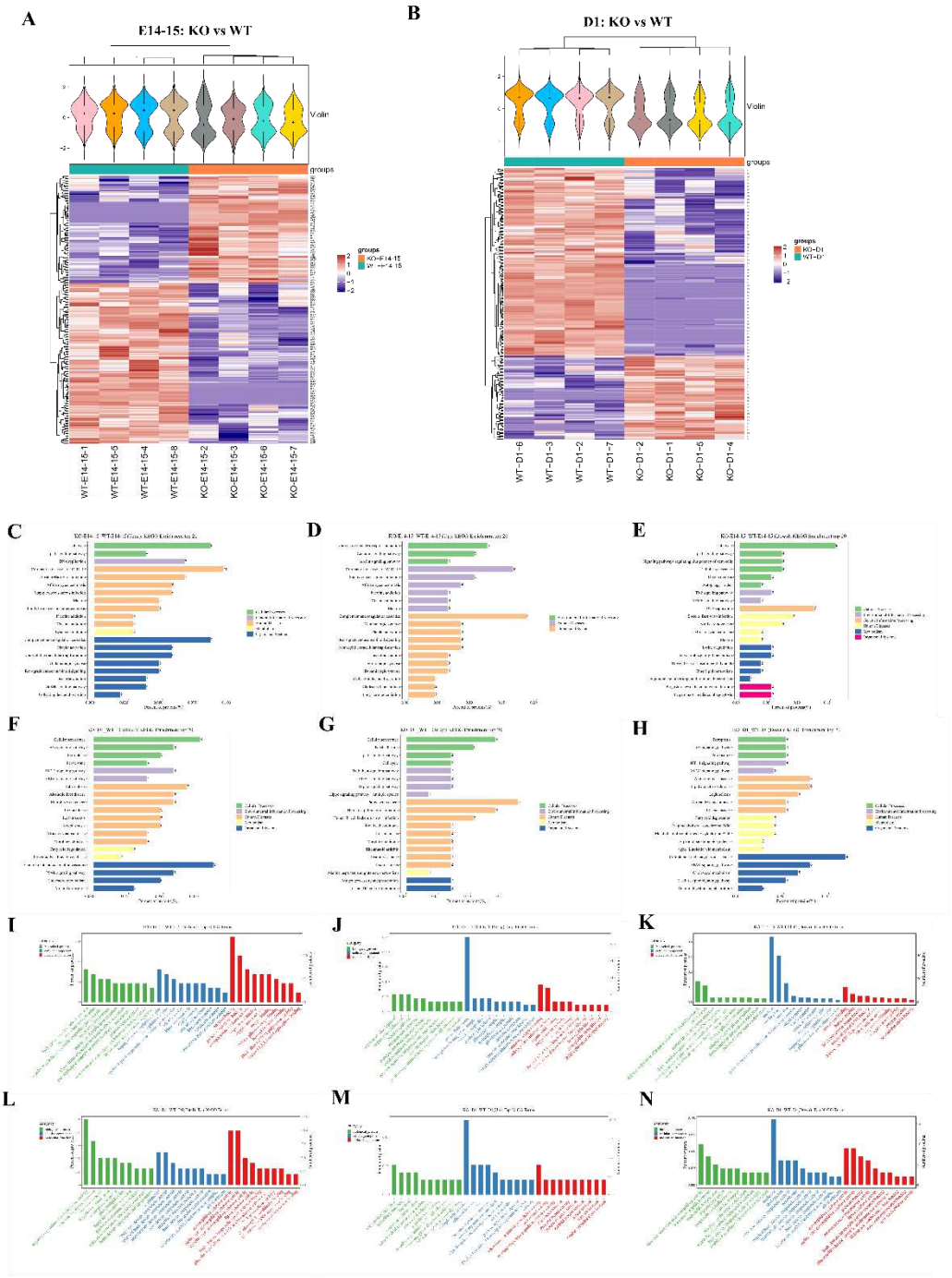


Fig.3. Proteomic profiling of mouse cerebral cortex at E14-15 and D1. A,B: Hierarchical clustering heatmaps of DEPs at E14-15 (A) and D1 (B). Rows represent proteins, columns represent biological replicates; color scale (blue to red) indicates relative expression (z-score). Violin plots above show sample expression distribution, colored by genotype. **C-H:** Top 20 KEGG pathway enrichment bar charts for distinct DEP subsets: total DEPs (C, F), upregulated DEPs (D, G), and downregulated DEPs (E,

H) in KO-E14-15_WT-E14-15 (C-E) and KO-D1_WT-D1 (F-H). Pathways are color-coded by functional category, and bar length corresponds to the enrichment percentage. **I-N:** Bar charts of top 30 significantly enriched GO terms for DEPs in indicated comparison groups, categorized into biological process (BP), cellular component (CC), and molecular function (MF). The x-axis represents the enrichment score (-log10(*P*-value)), and the right y-axis indicates the number of DEPs annotated to each GO term.

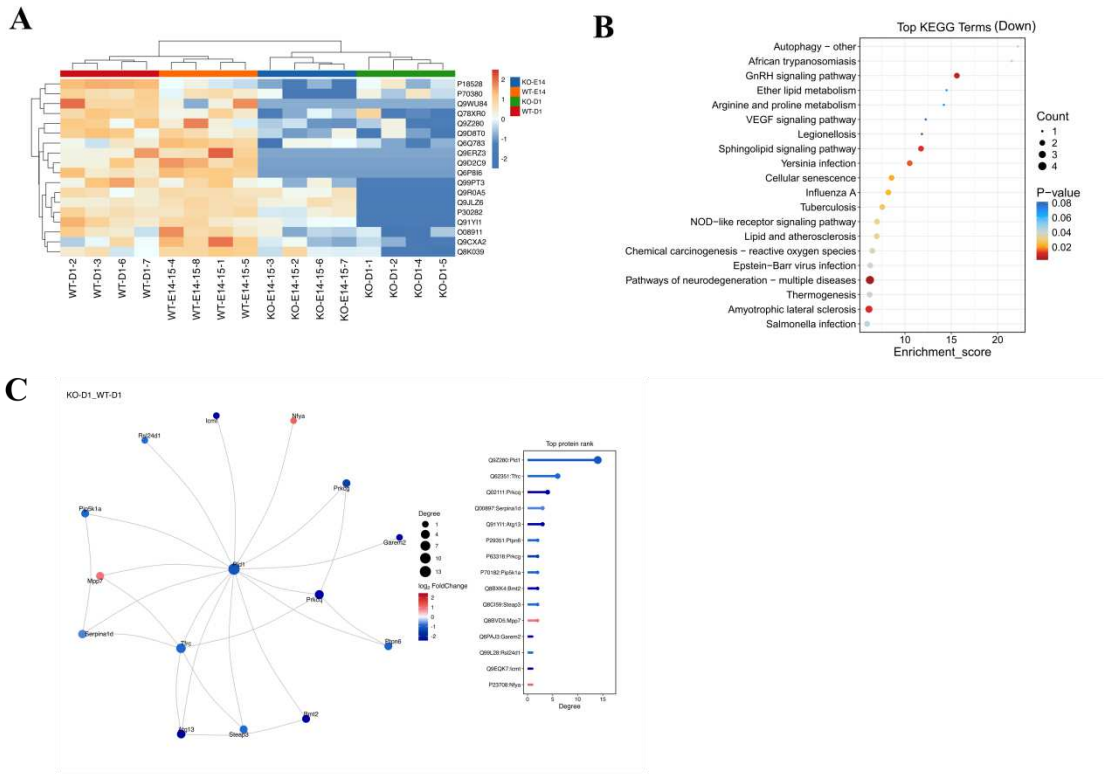


Fig. 4. Profiling of proteins consistently downregulated in KO-E14-15 and KO-D1, revealing key lipid metabolism hub protein PLD1. A: Hierarchical clustering heatmap of proteins downregulated in both KO-E14-15 and KO-D1. Rows represent proteins, columns represent biological replicates; color scale (blue to red) indicates relative expression (z-score). **B:** Top enriched KEGG terms of proteins downregulated in both KO-E14-15 and KO-D1. The x-axis represents enrichment score, the dot size corresponds to the number of enriched proteins (count), and the colour gradient indicates the *P*-value. C. PPI network of proteins downregulated in KO-D1 versus WT-D1. Node size represents the degree of connectivity; node colour indicates $\log_2$(fold change), with blue for downregulation and red for upregulation. The bar plot on the right shows the ranking of hub proteins based on degree.

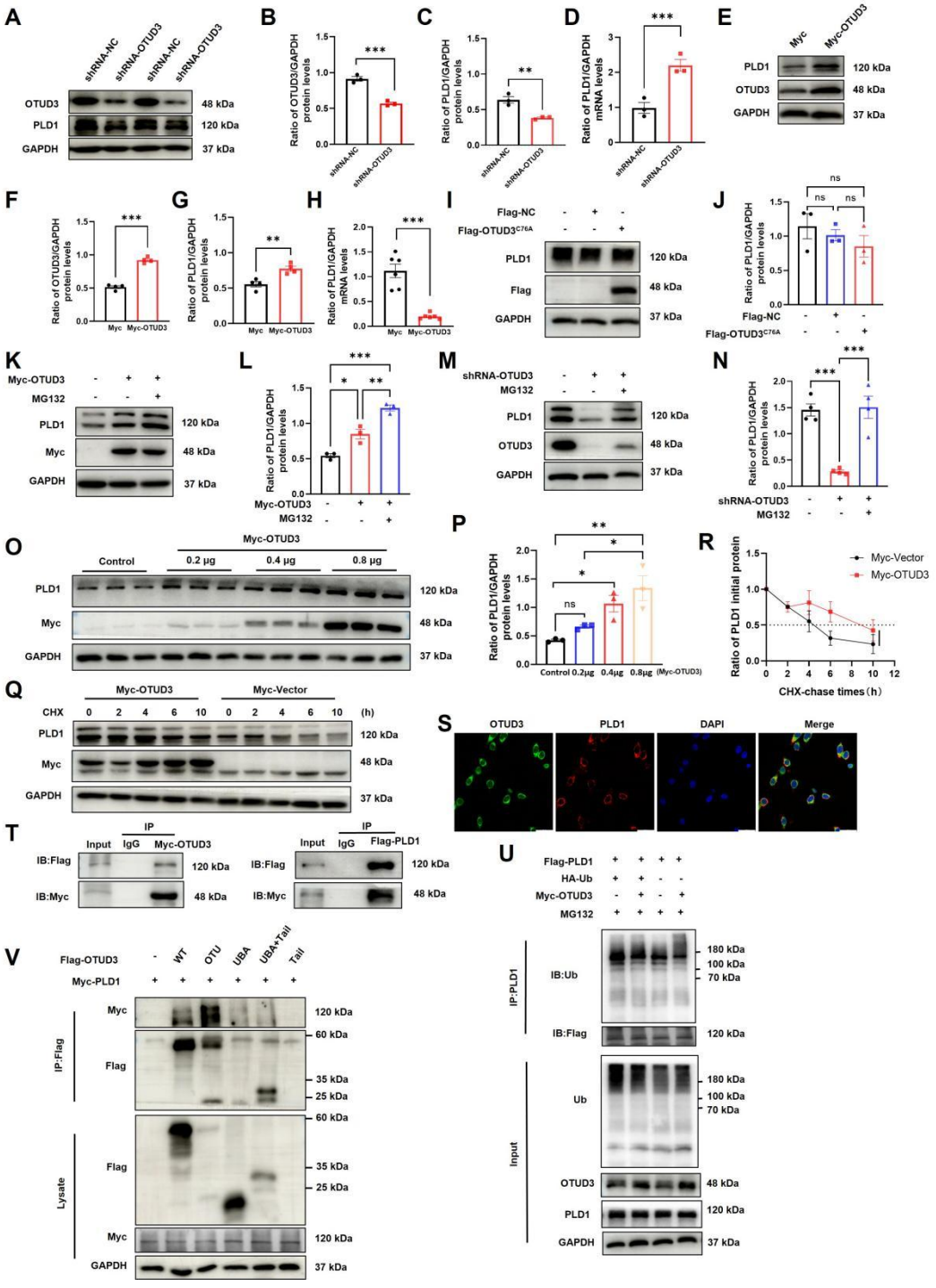


Fig. 5 OTUD3 interacts with PLD1 and stabilizes PLD1 protein through its deubiquitinase activity. A-D: Knockdown of OTUD3 reduces PLD1 protein level without affecting PLD1 mRNA expression in SH-SY5Y cells. Representative western blotting images (A), quantitative analysis of OTUD3 (B) and PLD1 (C) protein levels. qRT-PCR analysis of *PLD1* mRNA (D). **E-H:** Overexpression of Myc-OTUD3 increases endogenous PLD1 protein abundance, but *PLD1* mRNA levels decreased.

Representative immunoblot (E), quantitative statistics for OTUD3 (F) and PLD1 (G). qRT-PCR detection of *PLD1* transcripts (H). **I-J:** Catalytic-dead OTUD3^{C76A} mutant fails to upregulate PLD1 protein. Representative blots (I) and quantitative analysis (J). ns, not significant. **K,L:** Western blotting and quantitative analysis of PLD1 protein levels in cells transfected with Myc-OTUD3, with or without MG132 treatment. **M,N:** Western blotting and quantification of PLD1 in OTUD3-knockdown cells, with or without MG132. **O,P:** PLD1 protein accumulates in an OTUD3 dose-dependent manner. Western blot (O) and quantification (P). ns, not significant. **Q,R:** CHX-chase assay shows OTUD3 prolongs PLD1 protein half-life. Representative blots (Q) and quantitative decay curves (R). **S:** Immunofluorescence staining shows cytoplasmic co-localization of OTUD3 and PLD1. Scale bar=40 μm. **T:** Reciprocal Co-IP assays validate the physical interaction between OTUD3 and PLD1 in HEK293T cells. **U:** Ubiquitination assay showing wild-type OTUD3, but not OTUD3^{C76A}, decreases PLD1 ubiquitination. **V:** Domain-mapping Co-IP identifies the OTU domain of OTUD3 required for OTUD3-PLD1 interaction in HEK293T cells. All quantitative data are presented as mean ± SD. **P* < 0.05, ***P* < 0.01, ****P* < 0.001, ns: no significant difference. Student's t-test or one-way ANOVA was used for statistical analysis.

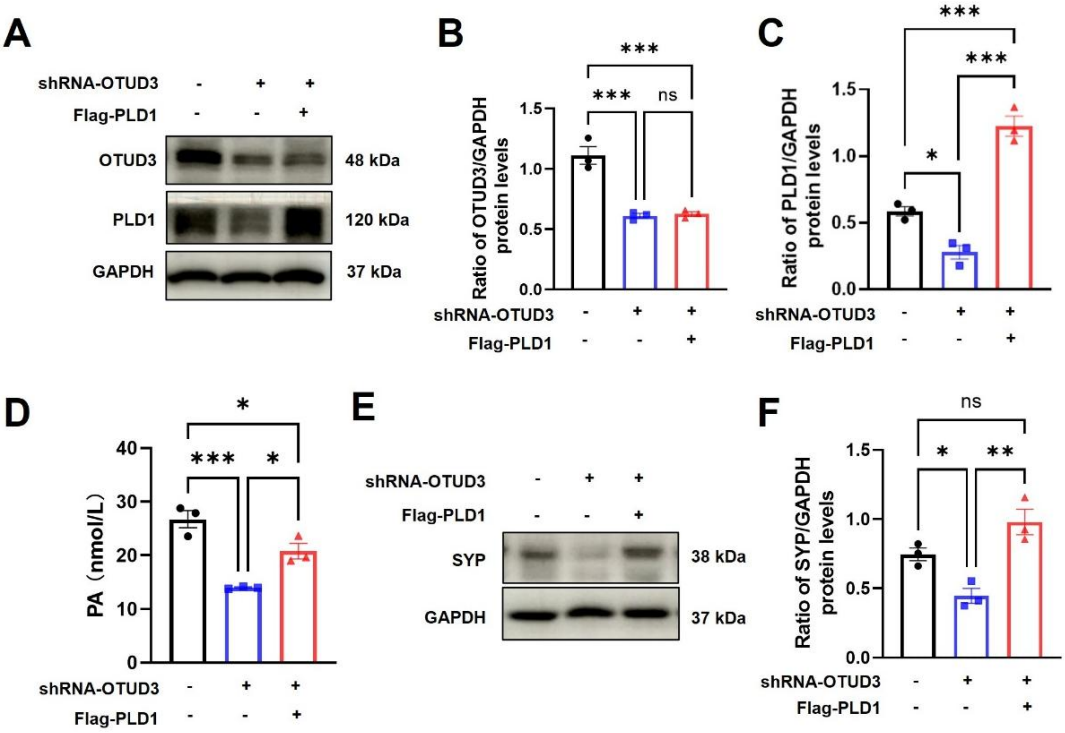


Figure 6. OTUD3-mediated PLD1 stabilization modulates PA production and SYP expression in SH-SY5Y cells. A: Representative western blotting images showing OTUD3, PLD1, and GAPDH protein levels in cells transfected with shRNA-OTUD3 and/or Flag-PLD1. **B,C:** Quantification of OTUD3/GAPDH (B) and PLD1/GAPDH (C) ratios from panel A. **D:** Quantification of PA levels in transfected cells. **E:** Representative western blotting images showing SYP and GAPDH protein levels. **F:** Quantification of SYP/GAPDH ratio from panel E. Data are presented as mean ± SD. * $P < 0.05$, ** $P < 0.01$, *** $P < 0.001$; ns, not significant.

Supplementary Files

This is a list of supplementary files associated with this preprint. Click to download.

- Supplementary.pdf
- table1.xlsx
- rawdata1015.pdf